Robust vortex lines, vortex rings, and hopfions in three-dimensional Bose-Einstein condensates

R. N. Bisset,[1,*] Wenlong Wang,[2] C. Ticknor,[3] R. Carretero-González,[4] D. J. Frantzeskakis,[5]
L. A. Collins,[3] and P. G. Kevrekidis[1,6]

[1]*Center for Nonlinear Studies and Theoretical Division, Los Alamos National Laboratory, Los Alamos, New Mexico 87545, USA*
[2]*Department of Physics, University of Massachusetts, Amherst, Massachusetts 01003, USA*
[3]*Theoretical Division, Los Alamos National Laboratory, Los Alamos, New Mexico 87545, USA*
[4]*Nonlinear Dynamical Systems Group,[†] Computational Sciences Research Center, and Department of Mathematics and Statistics, San Diego State University, San Diego, California 92182-7720, USA*
[5]*Department of Physics, University of Athens, Panepistimiopolis, Zografos, Athens 15784, Greece*
[6]*Department of Mathematics and Statistics, University of Massachusetts, Amherst, Massachusetts 01003-4515, USA*

(Received 15 October 2015; published 7 December 2015)

Performing a systematic Bogoliubov–de Gennes spectral analysis, we illustrate that stationary vortex lines, vortex rings, and more exotic states, such as hopfions, are robust in three-dimensional atomic Bose-Einstein condensates, for large parameter intervals. Importantly, we find that the hopfion can be stabilized in a simple parabolic trap, without the need for trap rotation or inhomogeneous interactions. We supplement our spectral analysis by studying the dynamics of such stationary states; we find them to be robust against significant perturbations of the initial state. In the unstable regimes, we not only identify the unstable mode, such as a quadrupolar or hexapolar mode, but we also observe the corresponding instability dynamics. Furthermore, deep in the Thomas-Fermi regime, we investigate the particlelike behavior of vortex rings and hopfions.

DOI: 10.1103/PhysRevA.92.063611 PACS number(s): 67.85.Bc, 03.75.−b, 47.32.cf

I. INTRODUCTION

Atomic Bose-Einstein condensates (BECs) have offered, over the last two decades, a fertile playground for the exploration of nonlinear matter waves [1–3]; for some recent summaries, see also Refs. [4–6]. While a large volume of the early work along this vein focused on solitons and vortices, the remarkable advancement of computational resources has rendered the frontier of three-dimensional (3D) structures more accessible. Arguably, the most prototypical among the latter, not only in superfluid but also in regular fluid settings [7,8], is the vortex ring (VR). VRs have not only been theoretically predicted, but also experimentally observed [3,4,9].

In addition to the VRs and vortex lines (VLs) extensively studied in earlier BEC experiments (see, e.g., Refs. [10,11] and a more recent experimental realization in Ref. [12]), BECs may support more complex topological structures, such as Skyrmions in multicomponent settings. In its simplest realization, originally proposed in Refs. [13,14], the Skyrmion consists of a VR in one component coupled to a VL in the second component. Interestingly, more complex Skyrmion states involving three-component spinor BECs were realized experimentally in both two [15] and three dimensions [16] involving, respectively, coupled states of topological charge $S=-1,0,1$ and $S=0,1,2$, and described in the recent theoretical work of Ref. [17]. Of increasing interest of late is the one-component counterpart to the Skyrmion, namely the so-called hopfion state [18,19]. This state consists of a VR and VL in the same component, with the axis of the VR coinciding with that of the VL. A stable hopfion state has so far only been predicted in somewhat complicated experimental configurations. These include, for instance, elaborate radially increasing nonlinear interactions [18] or a rotation of the trap [19]. Here we show that the hopfion can, in fact, be stable for large chemical potential ranges and simple trapping configurations, i.e., inside a parabolic trap.

Our main aim is to provide a systematic stability analysis of VRs, hopfions, and, in passing, VLs. By a detailed understanding of the pertinent modes of the Bogoliubov–de Gennes (BdG) linearization, we are able to explain when the relevant stationary states are stable or unstable. We also elucidate how such properties depend on geometric characteristics, such as the trap aspect ratio, and what instabilities one may encounter in different parameter intervals. These results should pave the way for the experimental identification of such coherent structures in state-of-the-art experimental setups of 3D BECs.

Our presentation is organized as follows. First, in Sec. II, we discuss the stability properties of the VR from an analytical perspective. Then, in Sec. III, we corroborate these analytical predictions of the relevant modes by means of highly intensive numerical spectrum computations. We thus show how the stability of the VR and the VL implies the potential stability of the hopfion pattern, and confirm this with our numerics. Furthermore, we provide an exploration of the unstable dynamics of the VR and hopfion states informed both by spectral properties and direct numerical simulations. Finally, in Sec. IV, we summarize our conclusions and discuss interesting directions for future studies.

II. ANALYTICAL CONSIDERATIONS

We begin with the 3D Gross-Pitaevskii equation (GPE),

$$i\hbar\frac{\partial\psi}{\partial t}=-\frac{\hbar^2}{2m}\nabla^2\psi+V(r)\psi+g|\psi|^2\psi, \tag{1}$$

where ψ is the wave function of the 3D Bose gas near zero temperature, $g=4\pi\hbar^2a_s/m$, with a_s being the s-wave

*rnbisset@gmail.com
†http://nlds.sdsu.edu

scattering length and m the particle mass. The potential assumes the prototypical form of the harmonic oscillator, $V(x,y,z) = m\omega_r^2 r^2/2 + m\omega_z^2 z^2/2$, with ω_r and ω_z being the planar and transverse trapping strengths, respectively. The case of $\omega_z > \omega_r$ leads to an oblate BEC, while the reverse inequality produces a prolate BEC.

In earlier work, following in the steps of, e.g., Ref. [20], we explored the bifurcation of a VR near the linear limit of low density, either from a planar or from a ring dark soliton [21]; here, our focus will be on the opposite limit. In particular, we consider the case of large chemical potential (small healing length), where the VRs can be considered as particlelike objects in their behavior and dynamics. Notice that in what follows, the chemical potential is used as a parameter, bearing in mind its one-to-one correspondence to the experimentally measurable number of atoms [1,2]. Reference [22], following the pioneering work of Ref. [23], explored the dynamics of the single VR in the presence of a trap. This is also examined in Ref. [24], where the results of Ref. [22] are utilized. In particular, the expression for the velocity of a vortex line element is given by

$$\mathbf{v}(\mathbf{x}) = \Lambda\left[\kappa\hat{\mathbf{b}} + \frac{\hat{\mathbf{t}}\times\nabla V}{F(r,z)}\right], \tag{2}$$

where $\Lambda = (-1/2)\ln(\sqrt{R_r^{-2} + \kappa^2/8}/\sqrt{2\mu})$ and κ denotes the curvature of the element; thus, for a VR $\kappa = 1/r$, while for a VL $\kappa = 0$. We denote by $\hat{\mathbf{b}}$ the binormal vector (for the axisymmetric VR, it is $\hat{\mathbf{z}}$), while $\hat{\mathbf{t}}$ denotes the tangent vector (equal to $\hat{\theta}$ for the VR). The quantity $F(r,z) = \max\{\mu - V(r),0\}$ represents the Thomas-Fermi (TF) density profile, relevant to the large density case, equivalent to large chemical potential, analyzed here; the corresponding radial and axial TF radii are given by $R_{r,z} = (2\mu/\omega_{r,z}^2)^{1/2}$. Note that Λ is accurate up to logarithmic corrections, which will be responsible for the approximate nature of the analytical results (in comparison to numerical findings) in what follows.

Assuming that $\Lambda(r)$ varies slowly with r (indeed logarithmically), the following equations of motion are then derived for a single VR inside the trap [24]:

$$\frac{1}{\Lambda(r)}\dot{r} = \frac{\omega_z^2 z}{F(r,z)},\quad \dot{\theta} = 0,\quad \frac{1}{\Lambda(r)}\dot{z} = \frac{-\omega_r^2 r}{F(r,z)} + \frac{1}{r}. \tag{3}$$

These equations predict the presence of an equilibrium radius of the VR in the $z = 0$ plane, i.e., $r_{\rm eq} = \sqrt{2\mu/(3\omega_r^2)}$. This effective radius seems to provide a natural generalization of the radius of the ring dark soliton [25,26], and is also in line with earlier results [27].

Reference [24] chiefly focused on considering the dynamics of azimuthal perturbations (Kelvin-wave-type modulations) using Eq. (2). In particular, they linearized around the stationary solution $(r,z) = (r_{\rm eq},0)$, using a perturbation of the form $r(t) = r_{\rm eq} + R_1(t)e^{in\phi}$ and $z(t) = Z_1 e^{in\phi}$, for integer n. Substitution of this linearization ansatz in Eq. (2) provides a generalized set of equations (Eqs. (5) and (6) in Ref. [24]) from which the effect of the azimuthal modulations on the motion of the VR can also be evaluated. Importantly, notice that this set of equations can account for the $n = 0$ oscillatory motion of the VR inside the trap, described by Eq. (3). The final result that we explore numerically in what follows is that the frequencies of vibration of the VR are given by

$$\omega = \pm\frac{3\Lambda(r_{\rm eq})\omega_r^2}{2\mu}\left[\left(n^2 - \frac{\omega_z^2}{\omega_r^2}\right)(n^2-3)\right]^{1/2}. \tag{4}$$

Importantly, we intend to test the ensuing implication that the VR stability depends on the shape of the condensate. More specifically, if the condensate is prolate ($\omega_z/\omega_r < 1$), then the VR should be unstable due to the $n = 1$ mode. If the condensate is spherical to slightly oblate ($1 \leqslant \omega_z/\omega_r \leqslant 2$), then at the particle level and under azimuthal perturbations, the VR and VL should be stable. Finally, for sufficiently oblate condensates, with $\omega_z/\omega_r > 2$, the VR should be unstable due to the $n = 2,\ldots,[\omega_z/\omega_r]$ modes, where the brackets denote the integer part function.

III. NUMERICAL RESULTS

A. Bogoliubov–de Gennes analysis

We start by considering the spectral linearization analysis around a stationary VR state, ψ_0. The relevant BdG ansatz will be of the form

$$\psi = e^{-i\mu t}\{\psi_0 + \epsilon[u(x,y,z)e^{i\omega t} + v^*(x,y,z)e^{-i\omega^* t}]\}, \tag{5}$$

where μ is the chemical potential, the asterisks denote complex conjugation, ϵ is a formal small parameter, and the presence of imaginary (or complex) eigenfrequencies ω reflects an instability along the direction of the corresponding eigenvector $(u,v)^T$.

In practice, we solve the GPE, given by Eq. (1), using a Newton-Krylov scheme [28]. For the BdG equations, we utilize the azimuthal symmetry of the trap in a way similar to Refs. [29,30]. This amounts to using spectral-basis modes that each have a definite angular momentum quantum number m proportional to $e^{im\phi}$. This way, we can treat the azimuthal variable analytically, effectively reducing the problem to 2D. Importantly, for a given excitation, the coupling between m subspaces is limited, and this allows the diagonalization of relatively small subsets independently. Specifically, if v of Eq. (5) resides in subspace m, then the u resides in subspace $m + 2s$, where s is the charge (angular momentum quantum number) of the stationary state [31].

Our fundamental premise in what follows is that for the large-μ regime, the spectrum of a state such as the VR or the VL consists of the union of two principal ingredients: the modes of vibration (undulation) of the VR or VL itself and the modes of the underlying TF ground state. Let us first analyze in more detail the BdG spectrum for the ground state of the system, and then progressively present results for VLs, VRs, and, finally, their hybrid, the hopfion. Note that the spectrum of the TF ground state has been identified early in Ref. [32] and the internal modes of the VR are described by Eq. (4).

Figure 1 depicts the BdG spectrum for the TF ground state of the system. Figure 1(a) depicts the spectrum for an isotropic (i.e., spherical) trap, $\omega_z/\omega_r = 1$, while Fig. 1(b) corresponds to an oblate trap, $\omega_z/\omega_r = 2.8$. The thick (blue) lines correspond to the numerical results, while the thin horizontal (black) lines correspond to the first few collective-mode excitations predicted by the theory [32]. It is clear from the figure that as the chemical potential μ increases, corresponding to a higher

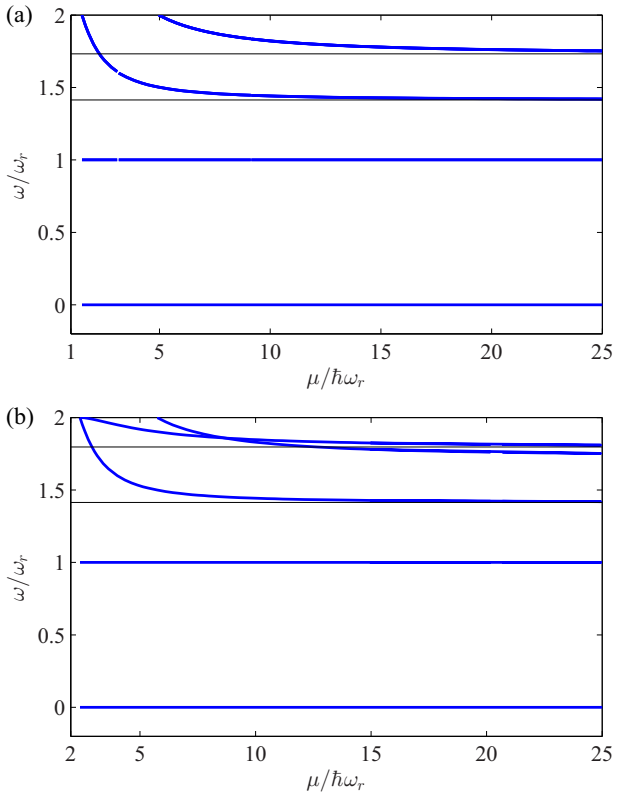

FIG. 1. (Color online) BdG-frequency spectrum for the ground state (bearing no vorticity) for (a) $\omega_z/\omega_r = 1$ and (b) $\omega_z/\omega_r = 2.8$. Stable (real) components are depicted by the thick blue lines. There are no unstable (imaginary) eigenvalues for the ground state. The thin horizontal lines pertain to the TF analytical predictions of Ref. [32].

number of atoms in the condensate, the full numerical spectrum coincides with the collective excitation frequencies prescribed by the theory.

Let us now turn to the BdG spectra for the VL and the VR. Figure 2 depicts the BdG spectrum for the VL in an isotopic trap, $\omega_z/\omega_r = 1$. Notice that modes corresponding to

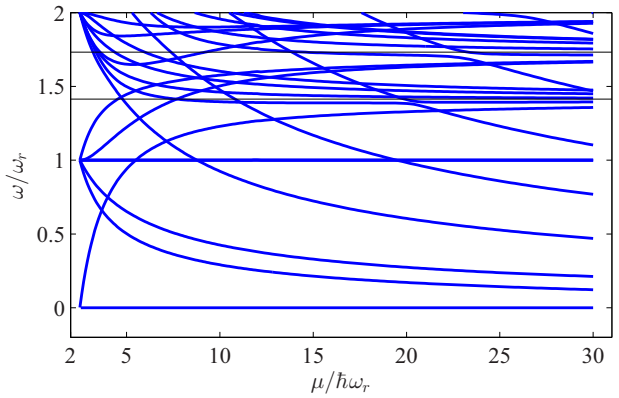

FIG. 2. (Color online) BdG-frequency spectrum for the VL in the isotropic $\omega_z/\omega_r = 1$ case. Stable (real) components are depicted by the thick blue lines. There are no unstable (imaginary) eigenvalues for this case. The thin horizontal lines pertain to the TF analytical predictions of Ref. [32] for the ground-state modes.

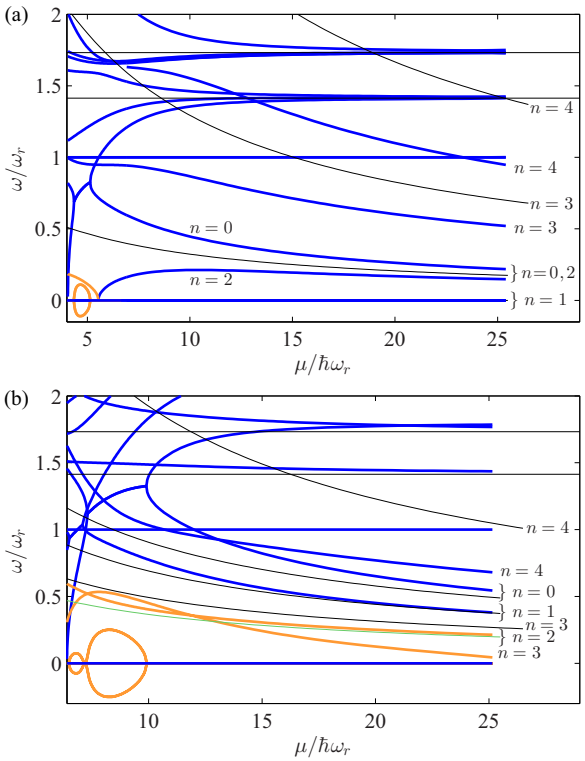

FIG. 3. (Color online) BdG-frequency spectrum for the VR for (a) $\omega_z/\omega_r = 1$ and (b) $\omega_z/\omega_r = 2.8$. Stable (real) components are depicted by the thick blue (dark) lines and unstable (imaginary) components by the thick orange (light) lines. Thin black lines correspond to the TF analytic predictions for (i) the VR [thin curved lines, Eq. (4)] and (ii) the ground state (thin horizontal lines; see Ref. [32]). The undulation number n [see Eq. (4)] of each excitation is indicated.

the ground state (see Fig. 1) are also contained in the spectrum of the VL and, as μ increases, one recovers again the collective excitations of the background prescribed by the theory [32]. It is also relevant to mention the observed spectral stability of the structure, given the absence of eigenfrequencies with an imaginary part. Figure 3 depicts the BdG spectra for the VR for $\omega_z/\omega_r = 1$ [Fig. 3(a)] and $\omega_z/\omega_r = 2.8$ [Fig. 3(b)]. As expected, we observe again the presence of the TF modes in the VR spectrum. The TF vibrational modes predicted in Ref. [32] correspond to the constant frequencies (thin horizontal lines), to which the relevant spectral modes approach asymptotically. On the other hand, the modes predicted by Eq. (4) feature a decay as $1/\mu$ (modulated by a logarithmic dependence). For the VR internal modes, the theoretical predictions, given by thin curved lines, reasonably approximate the numerical results, especially for larger values of μ. This approximation is especially good for the anomalous-vibration mode of the entire VR as a whole inside the trap ($n = 0$), as well as for undulations of the VR, such as the dipolar ($n = 1$) and quadrupolar ($n = 2$) modes. We note, however, that for higher-order modes, the analytical prediction of their frequency, based on Eq. (4), is less accurate. In the isotropic case of $\omega_z/\omega_r = 1$, the VR is expected to be generically stable in the large-μ limit, as predicted by Eq. (4), and indeed this is supported by our BdG analysis in Fig. 3. For small μ, however, the VR features

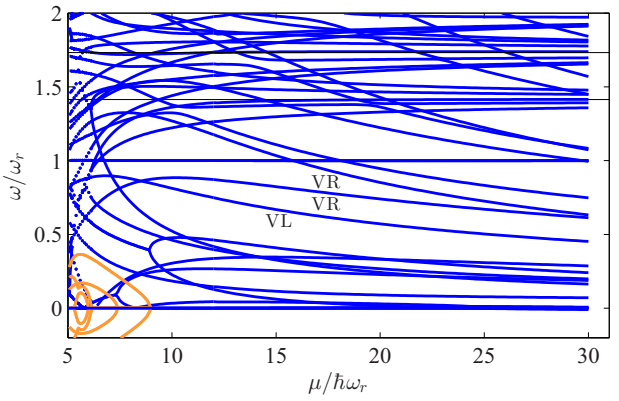

FIG. 4. (Color online) The spectrum of the hopfion with $\omega_z/\omega_r = 1$. The different types of curves have the same meaning as in Fig. 3. Importantly, we predict that the hopfion is stable for $\mu > 9$. While some excitations can be identified as strictly belonging to either the VR or the VL (see labeled examples), other excitations correspond to hybrid modes due to the coupling between the VR and the VL.

unstable modes, as described in detail in Ref. [21]. On the other hand, for $\omega_z/\omega_r = 2.8$, our results [cf. Fig. 3(b)] confirm that the VR is unstable due to the mode of $n = 2$ for all values of μ, as predicted by Eq. (4).

Having identified stable VRs and VLs in the isotropic limit for large μ suggests that the hopfion itself, consisting of a combined VR and VL in the same BEC, is likely to be stable in the TF limit. We have tested this prediction for $\omega_z/\omega_r = 1$ in Fig. 4: indeed, we observe that although instabilities may arise for small values of μ, for large values of μ the hopfion is robust. By investigation of the individual BdG eigenvectors, we find that the spectrum encompasses the union of VR, VL, and TF modes, with the analytical prediction for the latter [32] shown as thin horizontal lines. We have also labeled a few examples of purely VR and VL modes. However, we note that other modes demonstrate coupling between the VR and VL, as evidenced also by the hybrid nature of their BdG eigenvectors.

B. Nonlinear dynamics

To complement our spectral analysis, we explore the nonlinear dynamics of the VR and the hopfion, utilizing two methods. In the first, we temporally propagate the time-dependent GPE by employing a real-space product scheme, based on a split-operator approach, with the spatial component treated with a finite-element discrete-variable representation, using a Gauss-Legendre quadrature within each element [34]. For the second method, we use a split-step operator on a

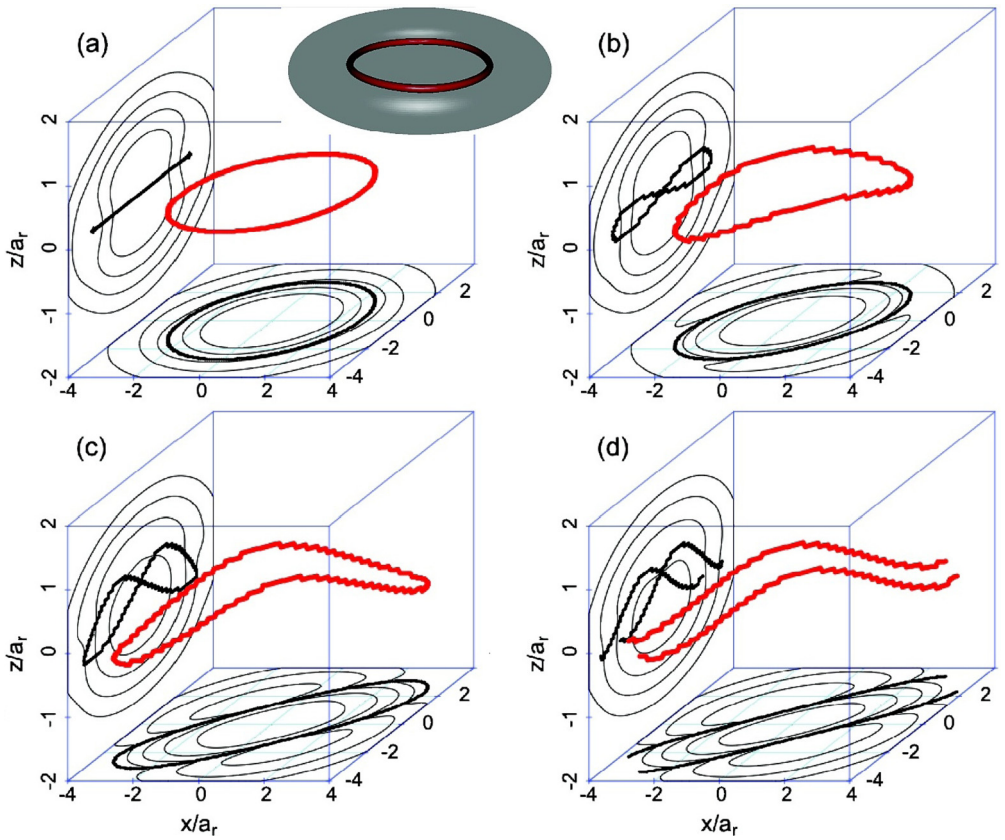

FIG. 5. (Color online) Dynamics of the VR, demonstrating instability to an $n = 2$ undulation, shown at times (a) $\omega_r t = 3.5$, (b) 25.4, (c) 29.0, and (d) 30.0. Parameters: $\omega_z/\omega_r = 2.8$ and $\mu/\hbar\omega_r \approx 15.3$. Red (gray) curves indicate vortex-core positions; thick black lines show the vortex-core projections onto the (x,y) and (y,z) planes; thin-black contour lines represent the column density projections at 0.2, 0.4, 0.6, and 0.8 of the peak. Inset: Isodensity surface of the stationary state at 0.1 of the peak; the inner isodensity surface of the VR is colored red. Units are that of the harmonic oscillator $a_r = \sqrt{\hbar/m\omega_r}$. To see a movie of the dynamics, see Ref. [33] (movie no. 1).

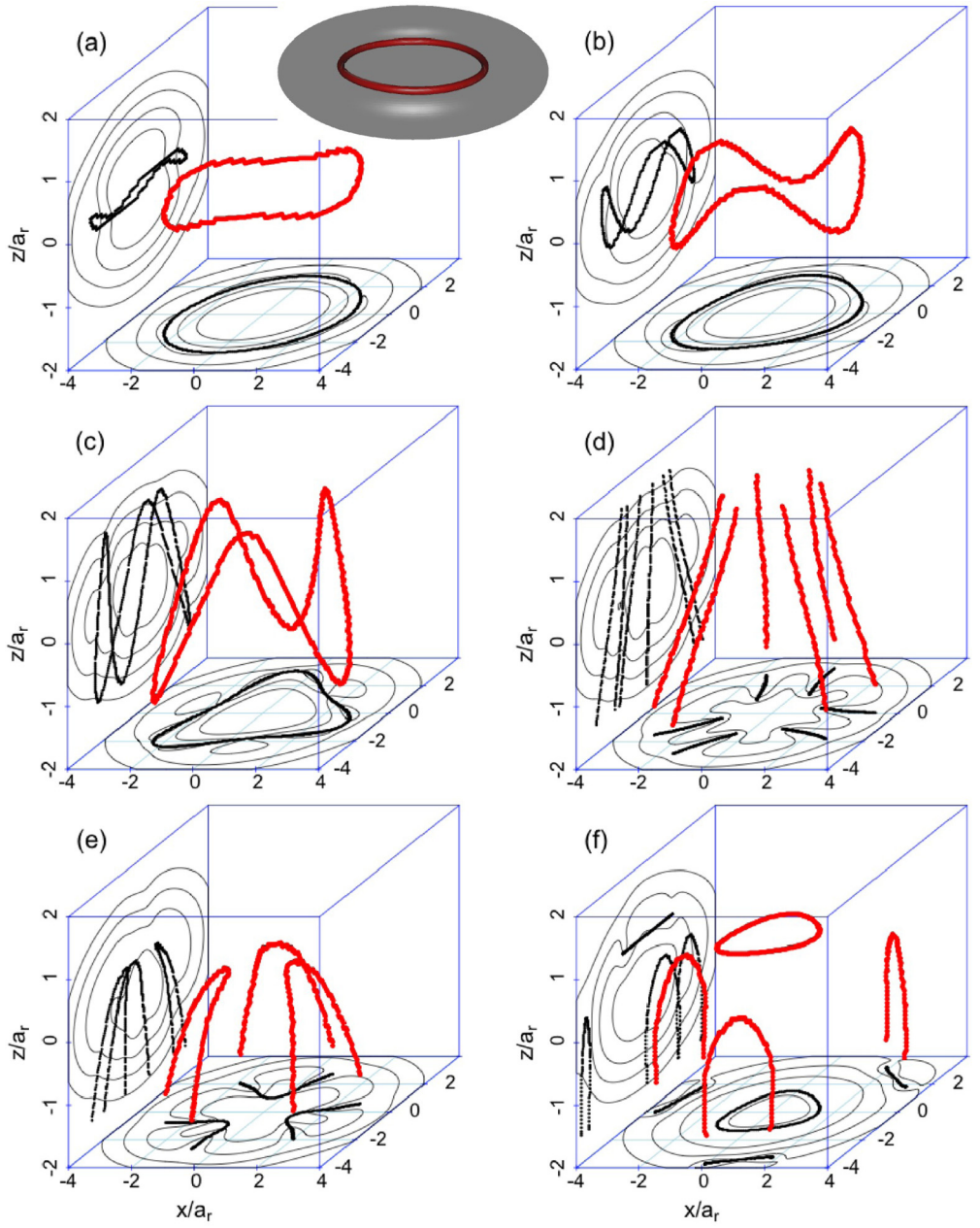

FIG. 6. (Color online) Demonstration of the VR instability to an $n = 3$ undulation, shown at times (a) $t\omega_r = 0$, (b) 4.9, (c) 7.4, (d) 8.4, (e) 9.4, and (f) 11.6. Same parameters and layout as in Fig. 5. To see a movie of the dynamics, see Ref. [33] (movie no. 2).

fast Fourier transform grid. For the results presented herein, we find quantitative agreement between these two numerical methods.

We first discuss the stability of the hopfion. At $\mu = 12$, where according to Fig. 4 the hopfion is stable, we performed two stability tests. In the first, we added an average of 1% random noise to ψ_0 on each grid point at time $\omega_r t = 0$, and found that the hopfion remains robust for the entire duration of the test, up to time $\omega_r t = 200$. In the second test, we excited the hopfion by adding a special excitation ψ_1 at the 5% level, i.e., $\psi_0 \to \psi_0 + 0.05\psi_1$, and found the hopfion to undulate in a stable manner for more than $\omega_r t = 200$ time units. Note that ψ_1 is the most unstable mode for small chemical potentials, $\mu/\hbar\omega_r < 9$ (see Fig. 4).

We now consider the instability dynamics. In Fig. 5, we examine the dynamics of the VR in a regime where it is found to be dynamically unstable in our earlier spectral analysis, in particular due to the $n = 2$ quadrupolar mode. As a result, we observe that the relevant (Kelvin) mode is amplified, until it eventually gives rise to the "rupture" of the VR into a pair of VLs. In Fig. 6, we also observe a similar dynamical evolution where the instability is seeded by the unstable $n = 3$ mode. In this case, the VR breaks into six VLs, before exhibiting a temporary revival of a smaller VR.

Finally, in Fig. 7 we examine the dynamical instability of the hopfion for $\mu \approx 7$, where it is still dynamically unstable prior to its stabilization for larger μ. The initial stages of the hopfion instability proceed in a similar manner to that

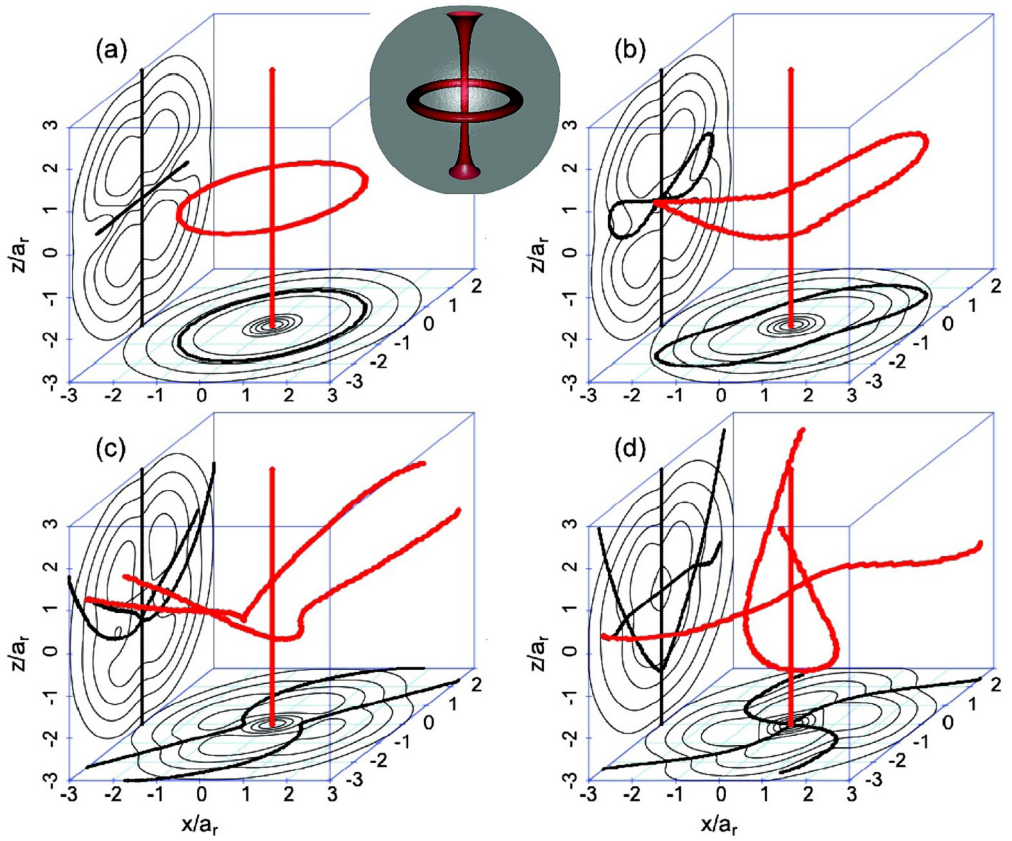

FIG. 7. (Color online) Dynamics of a hopfion instability at times (a) $\omega_r t = 0$, (b) 40.9, (c) 42.4, and (d) 44.3, after a random-noise seeding at $\omega_r t = 0$. Parameters: $\omega_z/\omega_r = 1$ and $\mu/\hbar\omega_r \approx 7.0$. Curves and contours have the same meanings as in Fig. 5. To see a movie of the dynamics, see Ref. [33] (movie no. 3).

of the VR. First, the VR part of the hopfion bends and then breaks into two VLs. The main difference arises when these VLs are subsequently pulled inwards to reconnect with the vertical VL. Interestingly, the VLs remain connected, with a "+" junction, for extended periods [see Fig. 7(d)]. Note that such reconnection events, particularly interesting in their own right and especially relevant in turbulent dynamics (see, e.g., Refs. [35,36]), have also been observed in the presence of rotation [19].

It is important to point out that the regimes considered in this work are experimentally accessible: for $\mu/\hbar\omega_r = 10.1$, a regime in which Fig. 4 predicts the hopfion to be stable corresponds to a ^{87}Rb BEC containing $\approx 1.1 \times 10^4$ atoms in an isotropic trap with $\omega_z = \omega_r = 2\pi \times 50$ Hz.

IV. CONCLUSIONS AND OUTLOOK

In the present work, we investigated 3D states that are supported in isotropic (and anisotropic) BECs. We used highly intensive numerical computations to explore their spectral stability, and found that the vortex line, vortex ring, and their combined state, the hopfion, are dynamically stable in a wide parameter regime. Importantly, we predict the hopfion to be robust in condensates within typical parameter regimes and standard trappings.

Our analysis not only identifies this stability, but also provides a road map on how to "decompose" the spectrum of these different states into its constituent parts (such as the excitations of the background, and the internal modes of the vortex ring and/or the vortex line) which, when combined, provide the full set of the observed excitation modes.

Both the analytical approach and our numerical computations explain why different trap aspect ratios may drastically affect the stability properties of such states. Finally, when the states were deemed to be unstable, direct numerical simulations elucidated their breakup and subsequent dynamics, such as the vortex line reconnections in the case of the hopfion.

An interesting future direction would be the extension of our investigations to a higher number of components: in particular, in the two-component setting, the analog of the hopfion would correspond to a Skyrmion, whose spectral and dynamical properties would be directly accessible through our approach. Another possibility would be to extend the considerations of some of the above structures to the attractive-interaction realm, examining their stability against collapse-type (and other) instabilities [37].

ACKNOWLEDGMENTS

We thank A. J. White for useful discussions. W.W. acknowledges support from the NSF (Grant No. DMR-1208046). P.G.K. gratefully acknowledges the support of NSF Grant No. DMS-1312856, of the ERC under FP7, Marie Curie Actions, People, International Research Staff Exchange Scheme (IRSES-605096) and insightful discussions with Professor

I. Danaila and Professor B. Malomed. R.C.G. gratefully acknowledges the support of NSF Grant No. DMS-1309035. The work of D.J.F. was partially supported by the Special Account for Research Grants of the University of Athens. This work was performed under the auspices of the Los Alamos National Laboratory, which is operated by LANS, LLC for the NNSA of the U.S. Department of Energy under Contract No. DE-AC52-06NA25396.

[1] C. J. Pethick and H. Smith, *Bose-Einstein Condensation in Dilute Gases* (Cambridge University Press, Cambridge, 2008).
[2] L. P. Pitaevskii and S. Stringari, *Bose-Einstein Condensation* (Oxford University Press, Oxford, 2003).
[3] *Emergent Nonlinear Phenomena in Bose-Einstein Condensates. Theory and Experiment*, edited by P. G. Kevrekidis, D. J. Frantzeskakis, and R. Carretero-González (Springer-Verlag, Berlin, 2008).
[4] P. G. Kevrekidis, D. J. Frantzeskakis, and R. Carretero-González, *The Defocusing Nonlinear Schrödinger Equation: From Dark Solitons, to Vortices and Vortex Rings* (SIAM, Philadelphia, 2015).
[5] V. S. Bagnato, D. J. Frantzeskakis, P. G. Kevrekidis, B. A. Malomed, and D. Mihalache, Rom. Rep. Phys. **67**, 5 (2015).
[6] D. Mihalache, Rom. J. Phys. **59**, 295 (2014).
[7] P. G. Saffman, *Vortex Dynamics* (Cambridge University Press, Cambridge, 1992).
[8] L. M. Pismen, *Vortices in Nonlinear Fields* (Clarendon, Oxford, 1999).
[9] S. Komineas, Eur. Phys. J. Spec. Topics **147**, 133 (2007).
[10] A. L. Fetter and A. A. Svidzinsky, J. Phys. Condens. Matter **13**, R135 (2001).
[11] A. L. Fetter, Rev. Mod. Phys. **81**, 647 (2009).
[12] D. V. Freilich, D. M. Bianchi, A. M. Kaufman, T. K. Langin, and D. S. Hall, Science **329**, 1182 (2010).
[13] J. Ruostekoski and J. R. Anglin, Phys. Rev. Lett. **86**, 3934 (2001).
[14] C. M. Savage and J. Ruostekoski, Phys. Rev. Lett. **91**, 010403 (2003).
[15] J. Y. Choi, W. J. Kwon, and Y. I. Shin, Phys. Rev. Lett. **108**, 035301 (2012).
[16] L. S. Leslie, A. Hansen, K. C. Wright, B. M. Deutsch, and N. P. Bigelow, Phys. Rev. Lett. **103**, 250401 (2009).
[17] J. Lovegrove, M. O. Borgh, and J. Ruostekoski, Phys. Rev. Lett. **112**, 075301 (2014).
[18] Y. V. Kartashov, B. A. Malomed, Y. Shnir, and L. Torner, Phys. Rev. Lett. **113**, 264101 (2014).
[19] Y. M. Bidasyuk, A. V. Chumachenko, O. O. Prikhodko, S. I. Vilchinskii, M. Weyrauch, and A. I. Yakimenko, Phys. Rev. A **92**, 053603 (2015).
[20] L.-C. Crasovan, V. M. Pérez-García, I. Danaila, D. Mihalache, and L. Torner, Phys. Rev. A **70**, 033605 (2004).
[21] R. N. Bisset, W. Wang, C. Ticknor, R. Carretero-González, D. J. Frantzeskakis, L. A. Collins, and P. G. Kevrekidis, Phys. Rev. A **92**, 043601 (2015).
[22] A. A. Svidzinsky and A. L. Fetter, Phys. Rev. A **62**, 063617 (2000).
[23] P. H. Roberts and J. Grant, J. Phys. A: Gen. Phys. **4**, 55 (1971).
[24] T.-L. Horng, S.-C. Gou, and T.-C. Lin, Phys. Rev. A **74**, 041603 (2006).
[25] G. Theocharis, D. J. Frantzeskakis, P. G. Kevrekidis, B. A. Malomed, and Yu. S. Kivshar, Phys. Rev. Lett. **90**, 120403 (2003).
[26] A. M. Kamchatnov and S. V. Korneev, Phys. Lett. A **374**, 4625 (2010).
[27] B. Jackson, J. F. McCann, and C. S. Adams, Phys. Rev. A **61**, 013604 (1999).
[28] C. T. Kelly, *Solving Nonlinear Equations with Newton's Method* (SIAM, Philadelphia, 2003).
[29] S. Ronen, D. C. E. Bortolotti, and J. L. Bohn, Phys. Rev. A **74**, 013623 (2006).
[30] P. B. Blakie, D. Baillie, and R. N. Bisset, Phys. Rev. A **86**, 021604(R) (2012).
[31] R. J. Dodd, K. Burnett, M. Edwards, and C. W. Clark, Phys. Rev. A **56**, 587 (1997).
[32] S. Stringari, Phys. Rev. Lett. **77**, 2360 (1996).
[33] We invite the interested reader to see the corresponding movies for the dynamics at this address: http://nonlinear.sdsu.edu/~carreter/Hopfion.html (unpublished).
[34] B. I. Schneider, L. A. Collins, and S. X. Hu, Phys. Rev. E **73**, 036708 (2006).
[35] A. J. Allen, S. Zuccher, M. Caliari, N. P. Proukakis, N. G. Parker, and C. F. Barenghi, Phys. Rev. A **90**, 013601 (2014).
[36] T. Wells, A. U. J. Lode, V. S. Bagnato, and M. C. Tsatsos, J. Low Temp. Phys. **180**, 133 (2015).
[37] B. A. Malomed, F. Lederer, D. Mazilu, and D. Mihalache, Phys. Lett. A **361**, 336 (2007).